Disturbance Observer Based Control Approach for Collaborative Robotics at Small Scales

Ahmad Awde[1,2], Mokrane Boudaoud[2], Stéphane Régnier[2], Cédric Clévy[1]

***Abstract*— Collaborative robotics allows merging the best capabilities of human and robots to achieve complex tasks. This enables the user to interact with distant and directly inaccessible environments such as the micro-scale world. This interaction is made possible through the bidirectional exchange of information (displacement-force) between the user and the environment through a haptic interface. The efficiency of the human/robot interaction strongly depends on how the human feels the forces. This is a key point to enable the human to take right decisions in a collaborative task. This paper deals with the design of a dynamic observer to estimate forces applied by a human operator on a class of parallel Pantograph type haptic interfaces used to control robotic systems at the small scales. The aim is to reject disturbances to improve the human force feeling capability in a wide frequency range. A dynamic model of a Pantograph is proposed and validated experimentally. The observer is designed based on the non linear dynamic model proposed and its efficiency for the estimation of the applied human force is for the first time demonstrated with Pantograph type interfaces. The experimental validation of the proposed approach shows firstly the effectiveness of the disturbance observer for the estimation of the external human force with a response time less than 0.2 s and a mean error less than 0.007 N and secondly the effectiveness of the controller to improve the quality of the force feedback sensing that can reached a variation of** 10 *mN* **.**

I. INTRODUCTION

Achieving efficient and safe robotic tasks at the small scales (1 nm-100 μm) in an automated or a tele-operated way is one of the main challenges of recent years. Several robotic systems with a high resolution, precision and flexibility are now available but they are not yet smart enough to deal with complex tasks [1]. For instance, the assembly of micro-mechanical components into a watch or the assembly for new integrated optical devices is often done by a human operator, which is able to adapt its operating mode when dealing with unpredictable situations. However, the human has not the required capabilities to deal with the physics at the small scales such as sensing forces at the micro-Newton and positioning the manipulation tool with a micrometer resolution. Micro-robotic systems are able to deal with such physical constraints but they are not able to make smart decisions. Collaborative robotics [2] is a key technology to improve the productivity of robotic tasks at the micro-scales. It merges the best capabilities of the human operator and the micro-robot to deal with complex manipulation and characterization tasks on micro- components and nano-materials.

[1]Univ. Bourgogne Franche-Comté, FEMTO-ST, UFC/CNRS/ENSMM, 24 rue Savary, 25000 Besancon, FRANCE ahmad.awde,cedric.clevy@femto-st.fr

[2]Sorbonne Université, Institut des Systèmes Intelligents et de Robotique, UMR 7222, ISIR, F-75005 Paris, France ahmad.awde, mokrane.boudaoud, stephane.regnier@sorbonne-universite.fr,

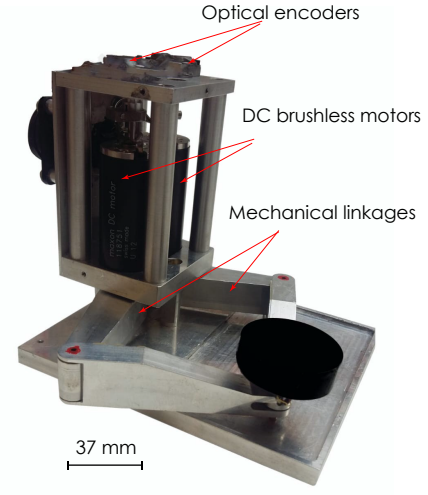

Fig. 1: Pantograph interface.

The collaboration between human and robot often referred as cobotics is characterized by a direct or an indirect interaction between human and robot to achieve a common goal. Many works on macro-scale robotics have shown the effectiveness of the collaborative approach to achieve tasks in industrial, military, agricultural and surgical [3] [4] [5] [6] [7] [8] fields. At the micro-scale, tele-operated and automated approaches have demonstrated their efficiency and complementarity in various applications such as micro-assembly [9] [10] [11] [12] [13] and biology [14] [15].

Usually, a micro-robot with a force sensing capability is coupled to a haptic interface. The latter is handled by a human operator and allows him to feel the forces applied by the micro-robot and to control the motion of the end effector [10] [16]. One of the main issues is that the force felt by the human is not only the force proportional to that returned by the micro-robot end effector, but also unwanted inertial and friction forces from the haptic interface as well as disturbance forces generated by the human himself. For a better transparency in the force feeling, these undesirable forces must be removed [17].

This paper focuses on human force estimation and disturbance rejection considering parallel type haptic interfaces for a fine human force feeling in a wide frequency

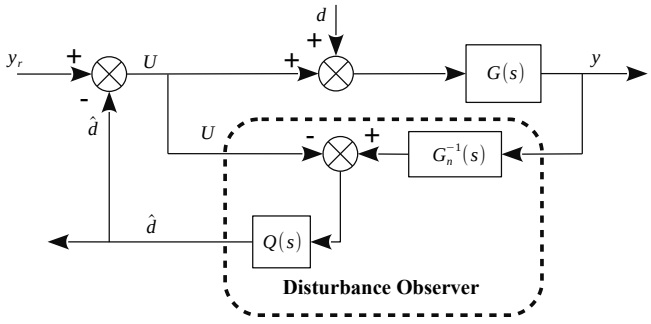

Fig. 2: Conceptual diagram of Disturbance Observer Based Control (DOBC) [20].

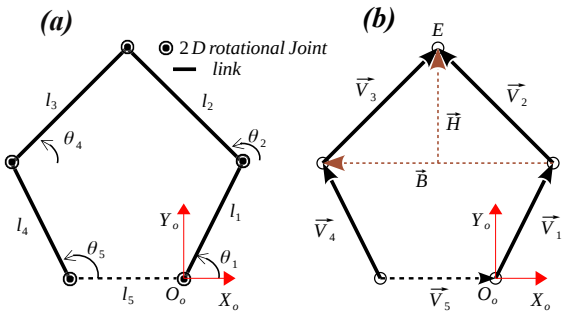

Fig. 3: Geometric representation for the kinematic study of the pantograph.

range. Such an issue is essential for an effective human decision making in a collaborative task. Parallel haptic interfaces are widely used in the fileds of robotics like Force Dimension's Omega®, SensAble's Phantom®. Such an architecture offers a low and high-frequency forces feeling to the human operator in range from the DC to the kHz [16].

In this study, we focus on *Pantograph* type architecture, initially reported in [18] [19], whose main advantage is that it has a uniform response over the entire human tactile frequency range [16]. The aim is to design a disturbance observer based on a dynamic model of the Pantograph which has never been reported in the literature. The observer aims at estimating the force applied by the human on the interface and to reject unwanted perturbations for better feeling of only the forces returned by the interface and proportional to that measured by a robot end effector. Several Disturbance-Observer-Based Control (DOBC) methods have been reported in the literature [20] but none of them have been designed and validated experimentally for Pantograph type interfaces. The basic architecture of the observer designed here [21] [20] is shown in Fig.2. To be used in the case of our study, a precise dynamic model $G(s)$ of the Pantograph is investigated in the paper to estimate the force applied by the human operator on the Pantograph in a dynamic way.

The remainder of this paper is organized as follows. The main architecture and features of the Pantograph studied in this paper are described in Section II. The kinematic modeling of the interface is presented in Section III. Section IV deals with the observed design considering the dynamic model and the control strategy. The experimental validations are presented in Section V. Finally, Section VI concludes the paper.

II. Pantograph

The architecture of the Pantograph is represented in Fig.1. It is mainly made of two DC bruchless motors, a kinematic chain and two optical Encoders. TABLE I resumes the essentials specifications of each component.

Fig. 3 and Fig. 4 show the kinematic representation of the Pantograph. The torques $[\tau_1, \tau_5]$ generated at the actives

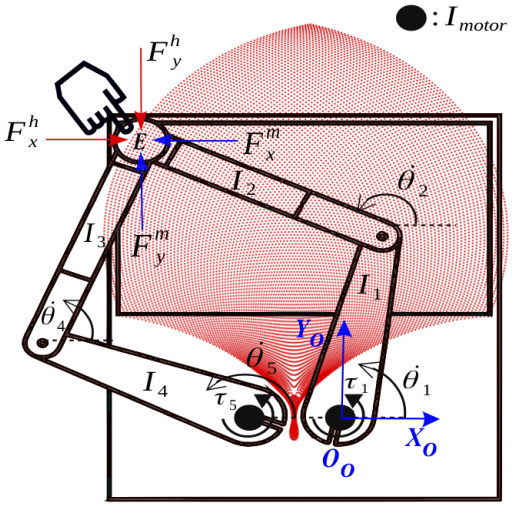

Fig. 4: Pantograph representation with its work-space.

joints 1 and 5 are transmitted to forces $[F_x^m, F_y^m]$ through the kinematic chain at end effector E . At E, the human operator senses the forces generated. By applying a forces $[F_x^f, F_y^h]$, the end effector moves and its position is tracked by measuring the rotational angle of the joints 1 and 5.

III. Kinematic and Dynamic Modeling

A. Kinematic Modeling

The kinematics problem consists on finding the position of the end effector E from the two measured joint angle θ_1 and θ_5 where the optical encoders are mounted (Fig. 3).

TABLE I: Pantograph components specifications

Component	Properties	Value
Brushless DC Motor Maxon RE 25	Power Nominal torque Rotor inertia I_{motor} Torque constant	20 W 24.2 mN.m 9.11 gcm^2 16.1 mN.m / A
MicroE systems Inc Optical Encoder	Resolution Max speed	100000 CPR 8640 RPM
Mechanical linkages	5 lightweight aluminium linkage	——

The origin frame $(O_oX_oY_o)$ is set at the first joint such as represented in Fig. 3 (b).
To solve this problem, each link j is represented by a vector $\overrightarrow{V}_j$ that connects its two joints where :

$$\begin{gathered} ||\overrightarrow{V_j}|| = \text{length of the link j} = l_j, \\ \arg \overrightarrow{V} = \text{orientation angle of the link} = \theta, \\ Z(\overrightarrow{V_j}) = l_j e^{i\theta}, j = 1,2,3,4,5 \end{gathered}$$

$Z(\overrightarrow{V_j})$ is the Euler representation of the complex number represented by the vector $\overrightarrow{V_j}$.

To obtain the position of the end effector E in the base reference, we should determine the vector $\overrightarrow{OE}$. After that, the coordinate of E can be expressed as :

$$\begin{aligned} Z(\overrightarrow{O_oE}) &= l_{OE} e^{i\theta_{OE}}, \\ &= l_{OE}\cos(\theta_{OE}) + i l_{OE}\sin(\theta_{OE}), \\ &= X_E + iY_E, \end{aligned} \tag{1}$$

Where l_{OE} and θ_{OE} are the length and the angle of orientation respectively of $\overrightarrow{OE}$. X_E, Y_E are the coordinate of E expressed in $(O_oX_oY_o)$.

Considering Fig. 3 (b) and taking into account that $||\overrightarrow{V}_2||$ and $||\overrightarrow{V}_3||$ are equal (because this two bars are equal), $\overrightarrow{OE}$ is calculated by a summation of vectors:

$$\begin{aligned} \overrightarrow{OE} &= \overrightarrow{V}_1 + 0.5\overrightarrow{B} + \overrightarrow{H}, \\ \overrightarrow{B} &= -\overrightarrow{V}_4 + \overrightarrow{V}_5 + \overrightarrow{V}_1, \end{aligned} \tag{2}$$

Where $\overrightarrow{H}$ is the perpendicular vector to $\overrightarrow{B}$.

Expressing (2) with the complex representation:

$$\begin{aligned} Z(\overrightarrow{OE}) &= Z(\overrightarrow{V}_1) + 0.5Z(\overrightarrow{B}) + Z(\overrightarrow{H}), \\ Z(\overrightarrow{B}) &= -Z(\overrightarrow{V}_4) + Z(\overrightarrow{V}_5) + Z(\overrightarrow{V}_1), \end{aligned} \tag{3}$$

With

$$\begin{aligned} Z(\overrightarrow{V}_1) &= l_1 e^{i\theta_1}, & Z(\overrightarrow{V}_4) &= l_4 e^{i\theta_5}, \\ Z(\overrightarrow{V}_5) &= l_5, & Z(\overrightarrow{H}) &= K e^{i\theta_H}, \\ K &= \sqrt{l_2^2 - (\tfrac{||\overrightarrow{B}||}{2})^2}, & \theta_H &= \arg(\overrightarrow{B}) - \tfrac{\pi}{2}, \end{aligned} \tag{4}$$

Finally, from (4) and (3) :

$$\begin{aligned} Z(\overrightarrow{OE}) &= 0.5(l_1 e^{i\theta_1} - l_5 + l_4 e^{i\theta_5}) + K e^{i\theta_H} \\ X_E &= \text{Real}(Z(\overrightarrow{OE})) \\ Y_E &= \text{Img}(Z(\overrightarrow{OE})) \end{aligned} \tag{5}$$

The Jacobian matrix can be found by a direct differentiation of the end effector E coordinates with respect to the actuated joints θ_1 and θ_5:

$$J = \begin{bmatrix} \partial X_E/\partial\theta_1 & \partial X_E/\partial\theta_5 \\ \partial Y_E/\partial\theta_1 & \partial Y_E/\partial\theta_5 \end{bmatrix}, \tag{6}$$

Equation (6) is used to map the joint-space torques onto the task-space forces as follows [22]:

$$F^m = J^{-T}\tau^m, \tag{7}$$

where $\tau^m \in \mathbb{R}^{2\times1}$ is the input torque vector presented in the joint space and $F^m \in \mathbb{R}^{2\times1}$ is the force vector representing the mapping of the input torques on the task-space forces.

Note : The rectangular shape of the work-space (see Fig. 4) is choosed to avoid the singularity of the Jaccobian matrix.

B. Dynamic Modeling

To obtain the dynamic equation of motion for the Pantograph, the *Euler-lagrange* method based on Fig.4 is used:

$$\frac{\partial}{\partial t}\left(\frac{\partial T}{\partial \dot{q}}\right) - \frac{\partial T}{\partial q} = Q \tag{8}$$

where T is the total energies of the system, q is the state variable vector $q = [\theta_1, \theta_2, \theta_4, \theta_5]'$ and Q is the total torque acting on the system (Motor input torque and the external human torque).

The haptic-device is a planar mechanism, the total energies is only the summation of the kinematic energies of each link T_i, $i = 1\ldots4$.

$$T = \sum_{i=1}^{4} T_i, \tag{9}$$

The kinetic energies of links (links 1 and 4) that exhibit rotational motion are given by :

$$T_1 = \tfrac{1}{2}(I_1 + I_{motor})\dot{\theta}_1^2 \quad \text{and} \quad T_4 = \tfrac{1}{2}(I_4 + I_{motor})\dot{\theta}_5^2 \ , \tag{10}$$

Links 2 and 3 undergoes translational and rotational motion. Therefore, their kinetic energy is given by:

$$\begin{aligned} T_2 &= \tfrac{1}{2}I_2\dot{\theta}_2^2 + \tfrac{m_2}{2}(l_1^2\dot{\theta}_1^2 + c_2^2\dot{\theta}_2^2 + l_1c_2\dot{\theta}_1\dot{\theta}_2 r21) \\ T_3 &= \tfrac{1}{2}I_3\dot{\theta}_4^2 + \tfrac{m_3}{2}(l_4^2\dot{\theta}_5^2 + c_3^2\dot{\theta}_4^2 + l_4c_3\dot{\theta}_5\dot{\theta}_4 r54) \end{aligned} \ , \tag{11}$$

where $r21 = \cos(\theta_2 - \theta_1)$ and $r54 = \cos(\theta_5 - \theta_4)$.

The mass m_i, the moment of inertia I_i and the distance to the center of mass c_i of each link are obtained using *SOLIDWORKS*. Results are shown in TABLE. II.

Based on (8), the dynamic equation of the haptic interface in the joint space is given by:

$$I_n(q)\ddot{q} + B_n(q,\dot{q})\dot{q} = \tau^m - \tau^{human} \tag{12}$$

where $I_n(q) \in \mathbb{R}^{4\times4}$ and $B_n(q,\dot{q})\dot{q} \in \mathbb{R}^{4\times4}$ are the inertia matrix and Coriolis damping matrix of the system in the joint space, respectively. Moreover, $\tau_m = [\tau_1, \tau_5]'$ and $\tau^{human} \in \mathbb{R}^{2\times1}$ are the motors torque input on the active joint and the human operator torque interaction with the Pantograph, respectively. In (12) $I_n(q)$ is given by

$$I_n(q) = \begin{pmatrix} I_{11} & I_{12} & 0 & 0 \\ I_{21} & I_2 + m_2c_2^2 & 0 & 0 \\ 0 & 0 & I_3 + m_3c_3^2 & I_{34} \\ 0 & 0 & I_{43} & I_{44} \end{pmatrix}, \tag{13}$$

TABLE II: PARAMETERS OF THE PANTOGRAPH.

link i	m_i	I_i	l_i	c_i
1	30.47 g	32469.88 gmm^2	63 mm	21.65 mm
2	14.01 g	27660.59 gmm^2	75 mm	38.04 mm
3	15.09 g	26780.93 gmm^2	75 mm	36.57 mm
4	30.47 g	32469.88 gmm^2	63 mm	21.65 mm
5	-	-	25 mm	-

where .

$$I_{11} = I_1 + I_{motor} + m_2 l_1^2, \quad I_{12} = I_{21} = \frac{m_2 l_1 c_2 r21}{2},$$
$$I_{44} = I_4 + I_{motor} + m_3 l_4^2, \quad I_{34} = I_{43} = \frac{m_3 l_5 c_3 r54}{2},$$

$B_n(q,\dot{q})$ is given by:

$$B_n(q,\dot{q}) = \begin{pmatrix} 2U_1\dot{\theta}_2 & -U_1\dot{\theta}_2 & 0 & 0 \\ U_1\dot{\theta}_1 & -2U_1\dot{\theta}_1 & 0 & 0 \\ 0 & 0 & 2U_2\dot{\theta}_5 & -U_2\dot{\theta}_5 \\ 0 & 0 & U_2\dot{\theta}_4 & -2U_2\dot{\theta}_4 \end{pmatrix}, \quad (14)$$

where

$$U_1 = \frac{m_2 l_1 c_2 \sin\theta_2 - \theta_1}{2}, \qquad U_2 = \frac{m_3 l_4 c_3 \sin\theta_5 - \theta_4}{2},$$

Therefore, we project the equation of motion onto the task-space to obtain

$$M_n(q)\ddot{x} + C_n(q,\dot{q})\dot{x} = F^m - F^{human}, \quad (15)$$

where $M_n(q) \in \mathbb{R}^{2\times2}$ and $C_n(q,\dot{q})\dot{q} \in \mathbb{R}^{2\times2}$ are the inertia and Coriolis damping matrix of the system expressed in the task-space. F^m is the forces vector generated by the motors at the end effector $F^m = J^{-T}\tau^m = [F_x^m, F_y^m]'$. F^{human} is the human input force vector $F^{human} = [F_x^h, F_y^h]'$.

A solution of each problem is proposed in [23], with $M_n(q)$ and $C_n(q,\dot{q})\dot{q}$ is given by

$$M_n(q) = \mathbb{J}^{-T} I_n(q) \mathbb{J}^{-1},$$
$$C_n(q) = \mathbb{J}^{-T} B_n(q) \mathbb{J}^{-1} - M_n(q)\dot{\mathbb{J}}\mathbb{J}^{-1}, \quad (16)$$

with $\mathbb{J} \in \mathbb{R}^{2\times4}$ a Jacobian matrix including the passive links of the haptic device and it is given by

$$\mathbb{J} = \begin{bmatrix} \partial X_E/\partial\theta_1 & 0 & 0 & \partial X_E/\partial\theta_5 \\ \partial Y_E/\partial\theta_1 & 0 & 0 & \partial Y_E/\partial\theta_5 \end{bmatrix}. \quad (17)$$

IV. Observer Design and Control

A. Instrumentation

The two DC motors are controlled with a current I. For this reason, A Quanser two-channel Linear Power Amplifier (LCA) is used. The purpose of using LCA is to ensure the current stability output I for a reference voltage input V with $I = \alpha V$ where α is the amplifying factor.

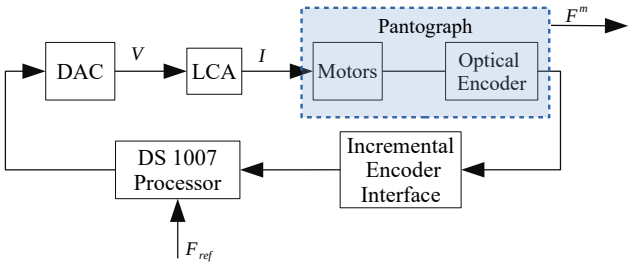

Fig. 5: Block diagram of the experimental component connection.

An Incremental Encoder Interface *DS*3001 is used to provide the absolute rotation angle from the output Optical Encoder signal.The Real-time control of the system is implemented using a DSpace *DS*1007 processor with Digital to Analog Converter *DAC DS*2102 that provide an analog output voltage signal. The instrumentation architecture to control the torque generation of the haptic-device is shown in Fig. 5.

B. Disturbance Observer Based Control

The Pantograph's dynamic equation of motion in the task-space is expressed in equation (15). From this equation, the human force applied on the haptic-device is:

$$F^{human} = F^m - M_n(q)\ddot{x} - C_n(q,\dot{q})\dot{x}, \quad (18)$$

According to Newton's third law, the human force sensation F_s^h is given by:

$$F_s^h = F^{human}. \quad (19)$$

From (18) and (19), if the desired force F_{ref} was applied directly on the system $F^m = F_{ref}$, we would have two situation:

- In static mode, $\dot{x} = 0$ and $\ddot{x} = 0$, the human senses only the force F^m,
- In dynamic mode, the influence of the inertia and Coriolis forces appears in the human force sensing.

If control input is calculated without considering the influence of the inertia and Coriolis forces, the human force sensing can be changed. For this reason, the control force input F^m of pantograph motors to be generated is developed to mask these influences and to have a uniform force sensation in dynamic like a static mode.

The aim of the control input F^m is to ensure that the human force sensing F_s^h is equal to the desired force F_{ref}. From (18) and taking $F^{human} = F_{ref}$, F^m can be obtained by

$$F^m = F_{ref} + \underbrace{M_n(q)\ddot{x}}_{F^{Inertia}} + \underbrace{C_n(q,\dot{q})\dot{x}}_{F^{Coriolis}}, \quad (20)$$

$F^{Coriolis}$ is calculated and fed back to cancel out the Coriolis force influence.

By feeding back the Coriolis force in the overall control F^m, (15) can be written as follows

$$M_n(q)\ddot{x} + \underbrace{F^{human}}_{\text{disturbance}} = F(t), \quad (21)$$

Here, we consider the human force F^{human} as an external disturbance. This disturbance can be estimated through the following filter [21]:

$$\hat{d} \approx \hat{F}^{human} = \frac{g}{s+g}(F + g \times M_n(q)\dot{x}) - g \times M_n(q)\dot{x}, \quad (22)$$

where $\hat{d}$ is the total estimated disturbance force, $\hat{F}^{human}$ is the estimated human force and g is the gain observer. In general, the selection of g should be large enough to cover the dynamical frequency range of the motion of the Pantograph. The observer output is the human force estimation that is

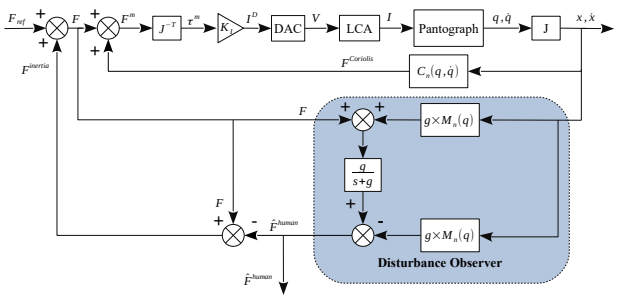

Fig. 6: Block diagram of the the global control scheme.

used to obtain an estimation of the inertia force $M_n(q)\ddot{x}$, where:

$$F^{Inertia} = M_n(q)\hat{\ddot{x}} = F - \hat{F}^{human}, \tag{23}$$

Therefore, $F^{Inertia}$ is added in the control input to eliminate the inertia force influence.

Fig. 6 rshows the global control block diagram of the Pantograph to improve the human sensing. The control input F^m is transformed into torques through the Jacobian matrix. The current I^D needed to ensure the torque control is obtained through the torque constant of the motors K_I. The digital current input I^D is converted into the analog one I using the *DCA* that controls the *LCA* with voltage signal.

V. Experimental validation

A. Force Generation

The aim here is to demonstrate that the reference force F_{ref} signal defined at the input of the controller (Fig. 6) is faithfully applied on the point E (Fig.4) of the pantograph. A Nano17 (SI-120.12) force sensor is used to measure the force F in y direction (i.e. F_y) generated by the Pantograph at the point E. Fig. 7 shows the experimental setup for the validation procedure. The block diagram of Fig. 6 is adopted to control the Pantograph. The results are represented in Fig. 8. Based on this results, The pantograph can generate forces with an error less than $0.007N$ and a response time $\approx 0.1s$.

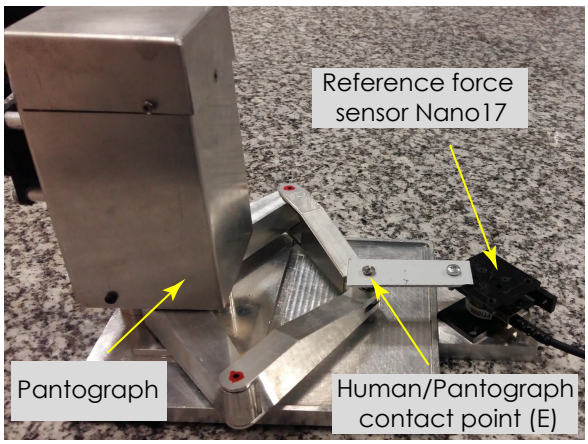

Fig. 7: Experimental setup for force measurement.

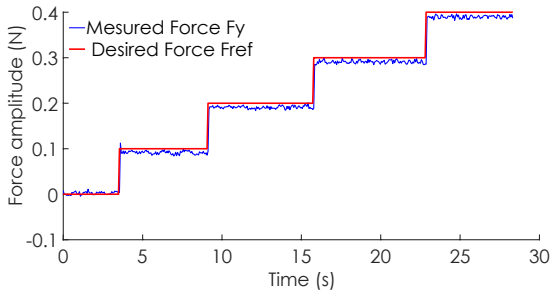

Fig. 8: Experimental measurement of the generated force by the Pantograph.

B. Observer Validation

After the validation of the forces generated by the Pantograph, the next step is to validate the DOBC output for our system without taking in consideration inertia force feedback.

Different values of F_{ref} have been applied to the Pantograph, namely 0.01 N, 0.05 N and 0.1 N without the presence of human operator on the haptic interface. Therefore, the observer must provide a signal that tends to zero in steady state. Fig. 9 shows the outputs of the DOBC for different input forces values.

From (15) and applying

$$F^m = F_{ref} + F^{Coriolis}, \tag{24}$$

the equation become

$$M_n(q)\ddot{x} = F_{ref} \tag{25}$$

In the absence of human operator, the pantograph moves freely. Only the control force F_{ref} and the inertia force $F^{inertia} = M_n(q)\ddot{x}$ are acting on the displacement of the system. The results presented in Fig 9 correspond well with our objectives. The DOBC applied is able to estimate an approximate zero human force interaction on the system $\hat{F}^{human} \approx 0$. Based on the disturbance output $\hat{F}^{human}$, the estimation of the inertia force is achieved $F^{Inertia} \approx F_{ref}$.

C. Human Force sensing

After the validation of the generated forces, the human force and the inertia force estimation through the DOBC, this section discusses the improvement of human force sensing.

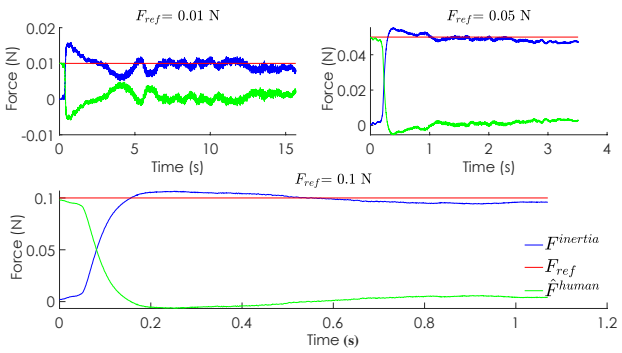

Fig. 9: Experimental Validation of the observer output.

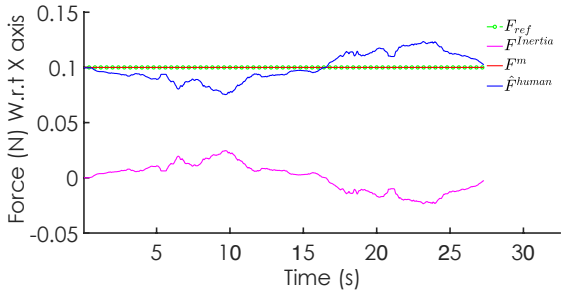

(a) The influence of the inertia force $F^{Inertia}$ on the human force feeling $\hat{F}^{human}$ with control force F^m ($F^m = F_{ref}$).

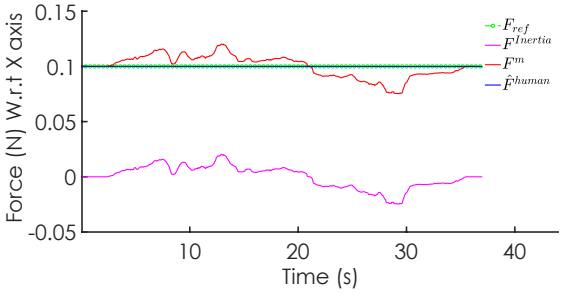

(b) The rejection of the inertia force influence $F^{Inertia}$ from the human force feeling $\hat{F}^{human}$ with control force F^m as (20).

Fig. 10: Comparison of the human force feeling with and without *Pantograph* dynamic rejection for low dynamic manipulation.

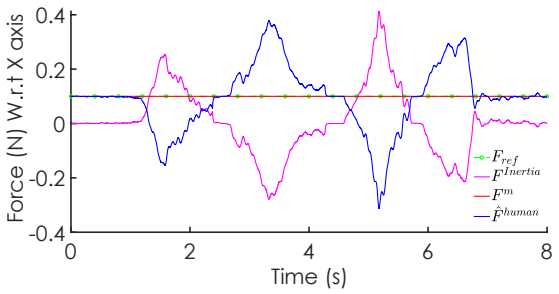

(a) The influence of the inertia force $F^{Inertia}$ on the human force feeling $\hat{F}^{human}$ with control force F^m ($F^m = F_{ref}$)

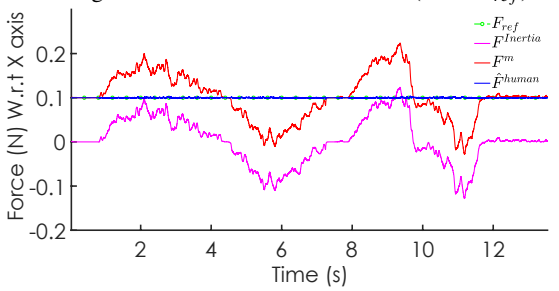

(b) The rejection of the inertia force influence $F^{Inertia}$ from the human force feeling $\hat{F}^{human}$ with control force F^m as (20).

Fig. 11: Comparison of the human force feeling with and without *Pantograph* dynamic rejection for high dynamic manipulation

As mentioned in Section IV-B, the human force sensation is affected by the dynamic of the haptic interface. For this reason, the block diagram represented in Fig. 6 is adopted to control the Pantograph in order to improve the human force feeling. The Figures 10 and 11 show a comparison of the human force feeling with and without taking into consideration the disturbance rejection for slow motion and speed motion applied by the human operator on the Pantograph. The human force feeling $\hat{F}^{human}$ is obtained from the DOBC (22).

Let us recall that the objective is that $F^{human} = F_{ref}$. The experimental results of Fig.10 are obtained for low dynamic motion of the human. In other words, when the human moves the pantograph at point E (Fig.4) slowly. It can be observed that without the observer based disturbance rejection (Fig.10 (a)), F^{human} is not equal to F_{ref}. With the disturbance rejection, the condition $F^{human} = F_{ref}$ is satisfied. Fig.11 demonstrate that the objective is also obtained when the human moves the pantograph with a faster motion. This is the first time in the literature that such a result is obtained for pantograph type haptic interfaces.

D. Positioning with respect force sensing

The perception of the human at its fingertip is limited to 10 mN [24]. This value changes from operator to another one and varies depending on various parameter such as temperature, humidity, sex , age, etc... .

The feeling of such force is affected by the inertial forces for low and high dynamic. In this section, we study the influence of the perturbation rejection on the positioning of pantograph with respect the force feed backed to the dynamic model for the pantograph. for this reason, the reference force is generated as follow :

$$F_{ref} = \begin{cases} F_{min} & \text{if } X_E \in [20,30] \cup [40,50] \cup [60,100] \ mm \\ 0 & \text{else.} \end{cases}$$

where F_{min} is the minimum force detectable by the human operator $F_{min} = 10\ mN$

The Figures 12 and 13 show a comparison for the human force feeling with and without taking into consideration the disturbances rejection for low and high dynamic respectively.

The Figures 12 and 13 show a comparison for the human force feeling with and without taking into consideration the disturbances rejection for low and high dynamic respectively.

Without perturbation rejection, For low and high dynamic, Fig. 12 -A- and 13 -A-, the inertia force $F^{Inertia}$ that act on the system dominate the force generated F_{ref}. For that, the human operator cannot distinguish the variation of the force which implies a difficulties to positioning with respect the force sensed. However, with the rejection of the perturbation, the inertia force is masked and the users can distinguish clearly the variation of the force on the specified position for a positioning with respect the force feeling.

VI. CONCLUSIONS

This paper has dealt with the dynamic modeling of a Pantograph type haptic interface and a Disturbance-Observer-

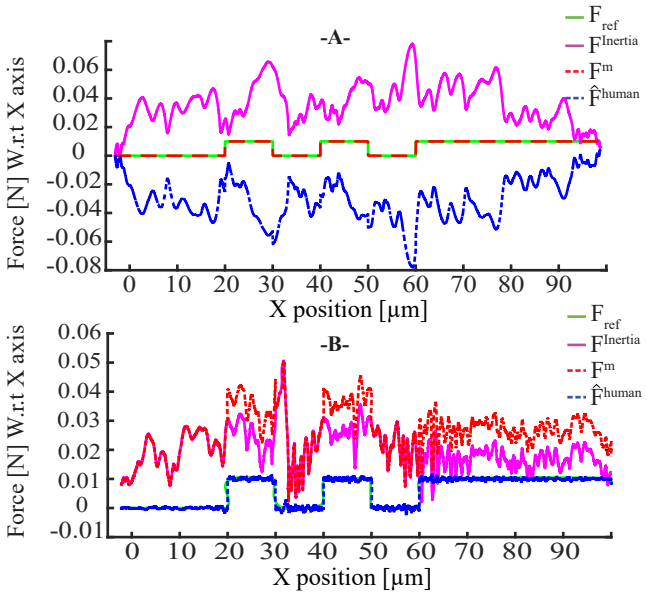

Fig. 12: Comparison for low dynamic manipulation of the positioning with respect the human force sensed **-A-** without Pantograph dynamic rejection **-B-** with Pantograph dynamic rejection.

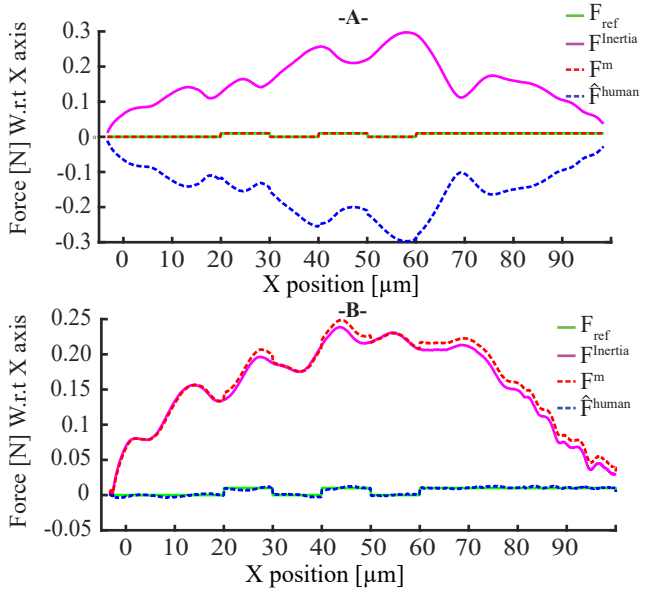

Fig. 13: Comparison for high dynamic manipulation of the positioning with respect the human force sensed **-A-** without Pantograph dynamic rejection **-B-** with Pantograph dynamic rejection.

Based Control (DOBC) to improve the human force feeling during a robotic collaborative task. A comprehensive dynamic model has been proposed and has been used to design the observer. Experimental validations have shown the effectiveness of such approach to estimate the external human force with response time less than 0.2 sec. The designed controller is able to reject unwanted perturbation forces due to the dynamic of the interface for low and high human dynamic inputs and achieved a feeling for a 10 mN variation of force (the limit for the human sensation). This result along with experimental validations has never been reported in the literature for Pantograph type interfaces. This is a key point to enable the human to take right decisions in a collaborative task.

ACKNOWLEDGMENT

This work was supported by the COLAMIR project (Contract "ANR-16-CE10-0009"), the Bourgogne Franche-Comté region, the EIPHI Graduate School (contract "ANR-17-EURE-0002"), and by the Robotex platform (Contract "ANR-10-EQPX-44-01").

REFERENCES

[1] J. Agnus, N. Chaillet, C. Clévy, S. Dembélé, M. Gauthier, Y. Haddab, G. Laurent, P. Lutz, N. Piat, K. Rabenorosoa, M. Rakotondrabe, and B. Tamadazte, "Robotic microassembly and micromanipulation at femto-st," *Journal of Micro-Bio Robotics*, vol. 8, pp. 91–106, Apr 2013.

[2] "Automotive assembly technologies review: challenges and outlook for a flexible and adaptive approach," *CIRP Journal of Manufacturing Science and Technology*, vol. 2, no. 2, pp. 81 – 91, 2010.

[3] V. Francoise, A. Sahbani, and G. Morel, "A comanipulation device for orthopedic surgery that generates geometrical constraints with real-time registration on moving bones," in *2011 IEEE International Conference on Robotics and Biomimetics*, pp. 38–43, 2011.

[4] C. P. Torterotot, M. Vitrani, P. Mozer, and G. Morel, "Ultrasound image-based comanipulation for enhanced perception of the contacts with a distal soft organ," in *2011 IEEE International Conference on Robotics and Biomimetics*, pp. 1140–1146, 2011.

[5] X. Lamy, F. Colledani, F. Geffard, Y. Measson, and G. Morel, "Achieving efficient and stable comanipulation through adaptation to changes in human arm impedance," in *2009 IEEE International Conference on Robotics and Automation*, pp. 265–271, 2009.

[6] J. M. Florez, J. Szewczyk, and G. Morel, "An impedance control strategy for a hand-held instrument to compensate for physiological motion," in *2012 IEEE International Conference on Robotics and Automation*, pp. 1952–1957, IEEE, 2012.

[7] T. Carlson and Y. Demiris, "Collaborative control for a robotic wheelchair: evaluation of performance, attention, and workload," *IEEE Transactions on Systems, Man, and Cybernetics, Part B (Cybernetics)*, vol. 42, no. 3, pp. 876–888, 2012.

[8] J. Rehbein, T. Wrütz, D. Hotze, and R. Biesenbach, "Collaborative control with industrial robots," in *2017 International Conference on Research and Education in Mechatronics (REM)*, pp. 1–4, IEEE, 2017.

[9] A. Bolopion and S. Régnier, "A review of haptic feedback teleoperation systems for micromanipulation and microassembly," *IEEE Transactions on Automation Science and Engineering*, vol. 10, no. 3, pp. 496–502, 2013.

[10] A. Bolopion, H. Xie, D. S. Haliyo, and S. Regnier, "Haptic teleoperation for 3-d microassembly of spherical objects," *IEEE/ASME Transactions on Mechatronics*, vol. 17, no. 1, pp. 116–127, 2012.

[11] B. Komati, A. Kudryavtsev, C. Clévy, G. Laurent, B. Tamadazte, J. Agnus, and P. Lutz, "Automated robotic microassembly of flexible optical components," in *2016 IEEE International Symposium on Assembly and Manufacturing (ISAM)*, pp. 93–98, Aug 2016.

[12] S. Bargiel, K. Rabenorosoa, C. Clévy, C. Gorecki, and P. Lutz, "Towards micro-assembly of hybrid moems components on a reconfigurable silicon free-space micro-optical bench," *Journal of Micromechanics and Microengineering (JMM)*, vol. 20, April 2010.

[13] M. Sitti and H. Hashimoto, "Two-dimensional fine particle positioning under an optical microscope using a piezoresistive cantilever as a manipulator," *journal of Micromechatronics*, vol. 1, no. 1, pp. 25–48, 2000.

[14] X. Fan, M. Sun, Z. Lin, J. Song, Q. He, L. Sun, and H. Xie, "Automated noncontact micromanipulation using magnetic swimming microrobots," *IEEE Transactions on Nanotechnology*, vol. 17, no. 4, pp. 666–669, 2018.

[15] J. Kuncová-Kallio and P. Kallio, "Lab automation in cultivation of adherent cells," *IEEE transactions on automation science and engineering*, vol. 3, no. 2, pp. 177–186, 2006.

[16] T. Lu, C. Pacoret, D. Hériban, A. Mohand-Ousaid, S. Régnier, and V. Hayward, "Kilohertz bandwidth, dual-stage haptic device lets you touch brownian motion," *IEEE Transactions on Haptics*, vol. 10, no. 3, pp. 382–390, 2017.

[17] A. Mohand-Ousaid, G. Millet, S. Régnier, S. Haliyo, and V. Hayward, "Haptic interface transparency achieved through viscous coupling," *The International Journal of Robotics Research*, vol. 31, no. 3, pp. 319–329, 2012.

[18] V. Hayward, J. Choksi, G. Lanvin, and C. Ramstein, "Design and multi-objective optimization of a linkage for a haptic interface," in *Advances in robot kinematics and computational geometry*, pp. 359–368, Springer, 1994.

[19] A. Dufresne, O. Martial, and C. Ramstein, "Multimodal user interface system for blind and "visually occupied" users: Ergonomic evaluation of the haptic and auditive dimensions," in *Human—Computer Interaction*, pp. 163–168, Springer, 1995.

[20] W. Chen, J. Yang, L. Guo, and S. Li, "Disturbance-observer-based control and related methods—an overview," *IEEE Transactions on Industrial Electronics*, vol. 63, no. 2, pp. 1083–1095, 2015.

[21] T. Murakami and K. Ohnishi, "Observer-based motion control-application to robust control and parameter identification," in *Proceedings 1993 Asia-Pacific Workshop on Advances in Motion Control*, pp. 1–6, IEEE, 1993.

[22] O. Khatib, "A unified approach for motion and force control of robot manipulators: The operational space formulation," *IEEE Journal on Robotics and Automation*, vol. 3, no. 1, pp. 43–53, 1987.

[23] B. Siciliano, L. Sciavicco, L. Villani, and G. Oriolo, *Robotics: modelling, planning and control*. Springer Science & Business Media, 2010.

[24] G. Millet, S. Haliyo, S. Regnier, and V. Hayward, "The ultimate haptic device: First step," in *World Haptics EuroHaptics conference and Symposium on Haptic Interfaces for Virtual Environment and Teleoperator Systems*, pp. 273–278, March 2009.